Chemical Science

EDGE ARTICLE

View Article Online
View Journal | View Issue

Cite this: *Chem. Sci.*, 2015, **6**, 4438

Crystallization-induced dual emission from metal- and heavy atom-free aromatic acids and esters†

Yongyang Gong,[a] Lifang Zhao,[a] Qian Peng,[b] Di Fan,[b] Wang Zhang Yuan,*[a] Yongming Zhang*[a] and Ben Zhong Tang[cd]

Received 23rd January 2015
Accepted 20th April 2015

DOI: 10.1039/c5sc00253b

www.rsc.org/chemicalscience

Pure organic materials exhibiting room temperature phosphorescence (RTP) have significant fundamental importance and promising optoelectronic and biological applications. Exploration of metal- and heavy atom-free pure organic phosphors, however, remains challenging because achieving emissive triplet relaxation that outcompetes the vibrational loss is difficult without metal or heavy atoms. In this contribution, in contrast to aggregation-caused quenching (ACQ) normally observed in conventional chromophores, a unique phenomenon of crystallization-induced dual emission (CIDE), namely, simultaneously boosted fluorescence and phosphorescence upon crystallization, is observed in a group of pure organic aromatic acids and esters at ambient conditions. Moreover, two triplet-involved relaxations of delayed fluorescence (DF) and phosphorescence are activated. Such efficient intrinsic emission from both singlet and triplet states in a single compound without employing metal or heavy atoms is suitable for a variety of fundamental research and applications.

Introduction

Room temperature phosphorescence (RTP) has aroused extensive interest because of its unique photophysical processes and promising applications in organic light-emitting diodes (OLEDs),[1] chemical and biological sensing,[2] bioimaging,[3] photovoltaic devices,[4] *etc.* So far, however, phosphorescence is essentially confined to inorganic compounds or organometallic complexes, such as platinum (Pt), iridium (Ir) and gold (Au) complexes,[1a,2d,5–7] as a result of the promotion of intersystem crossing (ISC) in organic ligands through the triplet metal-to-ligand charge-transfer state. Although pure organic luminogens can be more conveniently designed and tailored at much lower costs when compared to their inorganic and organometallic counterparts, they are generally believed to be unable to emit efficient RTP due to the following reasons:[8] (1) transitions between singlet and triplet states involving spin flips are quantum mechanically forbidden; (2) occasionally, these transitions become partially allowed due to such perturbations as spin–orbit coupling or vibrational coupling induced by carbonyl (C=O) groups, hetero atoms and heavy atoms, active intramolecular motions and/or interacting with environmental quenchers can effectively extinguish the phosphorescence during the longevity of triplet excitons. Triplet states in organic luminogens are thus typically dark states. Although previous examples of solid substrate-RTP (SS-RTP),[9] micelle stabilized-RTP (MS-RTP)[10] and cyclodextrin-induced RTP (CD-RTP)[11] have been reported, normally special and complex fabrication techniques are required and only instrument detectable signals are obtained.

In 2010, we observed a new phenomenon of "crystallization-induced phosphorescence (CIP)" in pure organic luminogens, namely, compounds like benzophenone and its derivatives are nonphosphorescent in solutions and amorphous states, while being efficiently phosphorescent upon crystallization.[12] The discovery of CIP affords a crystal engineering approach to obtain efficient RTP. The mechanism of CIP is ascribed to the restriction of intramolecular motions (RIM) by effective intermolecular interactions in the crystals, which help to lock and rigidify the molecular conformations, thus minimizing the nonradiative loss of triplet excitons and boosting the phosphorescence emission.[12] Meanwhile, crystalline lattices also prevent the luminogens from contacting with such quenching sites as oxygen and moisture.[13]

Later, Kim and co-workers found a similar phenomenon resulting from directed heavy atom effect (DHAE) in the aromatic aldehyde and bromide cocrystals.[14] Subsequently, other examples of RTP based on pure organic luminogens have been reported by taking advantage of (co)crystallization,

[a]*Shanghai Key Lab of Electrical Insulation and Thermal Aging, School of Chemistry and Chemical Engineering, Shanghai Jiao Tong University, Shanghai 200240, China. E-mail: wzhyuan@sjtu.edu.cn; ymzsjtu@gmail.com*

[b]*Institute of Chemistry, Chinese Academy of Sciences, Beijing 100190, China*

[c]*Department of Chemistry, The Hong Kong University of Science & Technology, Clear Water Bay, Kowloon, Hong Kong, China*

[d]*HKUST-Shenzhen Research Institute, No. 9 Yuexing 1st RD, South Area, Hi-tech Park, Nanshan, Shenzhen 518057, China*

† Electronic supplementary information (ESI) available. CCDC 1044990 and 1044991. For ESI and crystallographic data in CIF or other electronic format see DOI: 10.1039/c5sc00253b

halogen bonding, doping in rigid matrix, intermolecular interaction and singlet fission.[15–19] Efficient pure organic RTP luminogens, however, remain rather limited,[10–21] particularly for those without heavy atoms.

With continuous endeavors to construct pure organic phosphors with efficient RTP,[21] in this work, we report on the efficient crystal emission from both singlet and triplet manifolds in a group of metal- and heavy atom-free aromatic acids and esters (Chart 1). Recently, Reineke and co-workers also reported the impressive work of efficient bioluminescence (fluorescence and phosphorescence) from *N*,*N*′-bis(4-benzoylphenyl)-*N*,*N*′-diphenyl-benzidine [(BzP)PB] embedded into a polymethyl methacrylate (PMMA) film.[19b] (BzP)PB is emissive in both solutions and solids, but suffers from an aggregation-caused quenching (ACQ) problem (Fig. S2, ESI†); moreover, no RTP is observed in its crystals (Fig. S3, ESI†). Distinctly different from (BzP)PB, our acids and esters are practically non-emissive in solutions and on TLC plates, however, they emit both fluorescence and phosphorescence upon crystallization, demonstrating crystallization-induced dual emission (CIDE) characteristics, which enable the possibility to quantify singlet–triplet spin correlations.[22] Moreover, besides normal prompt fluorescence and phosphorescence, delayed fluorescence (DF) is also detected. Such CIDE feature not only eliminates the troublesome procedures normally adopted to observe phosphorescence at cryogenic temperatures, but also avoids the concentration quenching that is popular and particularly strong for long-lived triplets.[23]

Results and discussion

For pure organic luminogens, to achieve efficient RTP, it is essential to promote spin–orbit coupling to enable efficient ISC to the triplet state and to suppress the vibrational dissipations. Herein, aromatic acids were chosen based on the following considerations: firstly, carbonyl groups can effectively enhance spin–orbit coupling and thus ISC process;[24] secondly, acids readily form strong and effective intermolecular interactions such as hydrogen bonds in the condensed states,[25] which can significantly impede the nonradiative depopulation of triplet excitons. As a typical aromatic diacid, terephthalic acid (TPA) was first investigated. In oxygen-free ethanol, TPA emits UV light with the maximum at 319 nm in a low solution efficiency (Φ_s)[26] of 0.57 ± 0.07%, indicating it is practically nonluminescent. When dotted on a TLC plate, also no emission is observed (Fig. S4, ESI†).

The low photoluminescence (PL) efficiency of TPA in solutions and disordered amorphous states should be ascribed to the active vibrational and rotational dissipations.[12,14,21b] Unlike these solutions and disordered solids, crystalline powders of TPA exhibit intense deep blue emission (388 nm, Fig. 1A and B) with the crystalline efficiency (Φ_c)[26] of 8.4 ± 0.3%. With the delay time (t_d)[27] of 0.5 ms, no signal is recorded for the solution emission, whereas a peak (392 nm) and a shoulder (511 nm) assignable to DF and RTP are observed for the crystal emission. Further transient PL measurement reveals the presence of both short- and long-lived species with lifetimes ($\langle\tau\rangle$) of 0.53 ns and 0.16 ms (monitored at 380 nm, Fig. 1C), indicating the coexistence of prompt fluorescence and DF for the crystal emission. These results clearly suggest the CIDE characteristics of TPA, which is seldom observed in pure organic luminogens. Notably, DF of TPA crystals is slightly red shifted compared to that of the prompt spectrum, which is also observed in other systems.[28] Though the exact mechanism remains an open question, it is suggested that the red-shift of DF is caused by the difference in nuclear configuration in the singlet and triplet excited states.[28b]

Isomeric effect and fluorine atom will impact on the electron distribution, thus yielding varied photophysical properties. In analogy to TPA, isophthalic acid (IPA) and tetrafluoroterephthalic acid (TFTPA) are almost nonluminescent in solutions, showing fluorescence emissions at 305 and 307/367 nm with even lower Φ_s values of 0.33 ± 0.09% and 0.30 ± 0.03%. Their crystals, however, emit strong blue light upon UV illumination (Fig. 2A, B and 3A) with emission maxima/Φ_c values of 380 nm/15.3 ± 0.3% and 367 nm/2.0 ± 0.3% for IPA and TFTPA (Fig. 2D and 3B), respectively. Moreover, a long green afterglow lasting for several seconds is detected for IPA crystals after photoexcitation is stopped (Fig. 2C and Video S1, ESI†), which is attributable to the RTP emission. Such bright and persistent RTP from pure organic compounds is rarely found and makes the IPA crystals highly applicable in security inks, optical sensing, background-independent bioimaging and other optoelectronic devices.[2a,18,20] With a time-gated technology, independent emission peaks at 384/506 (IPA, t_d = 10 ms, Fig. 2D) and 367/484 nm (TFTPA, t_d = 0.1 ms, Fig. 3B) are observed. While the shorter wavelength emission can be attributed to DF,

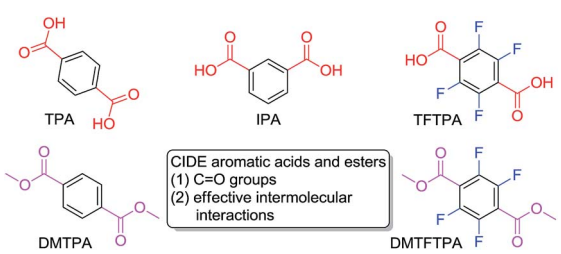

Chart 1 Structure of aromatic acids and esters with CIDE characteristics studied in this work.

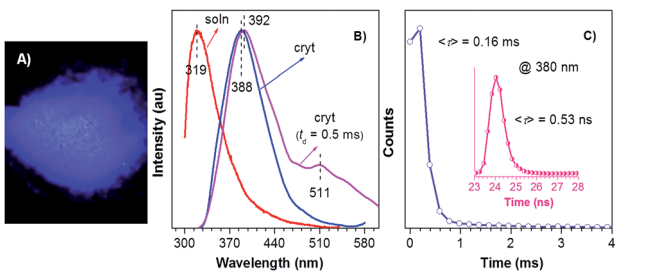

Fig. 1 (A) Photograph of crystalline powders of TPA taken under 365 nm UV light. (B) PL spectra of TPA solution (20 μM in ethanol) and crystalline powders with t_d of 0 and 0.5 ms. (C) Emission decay curves of crystalline powders of TPA monitored at 380 nm.

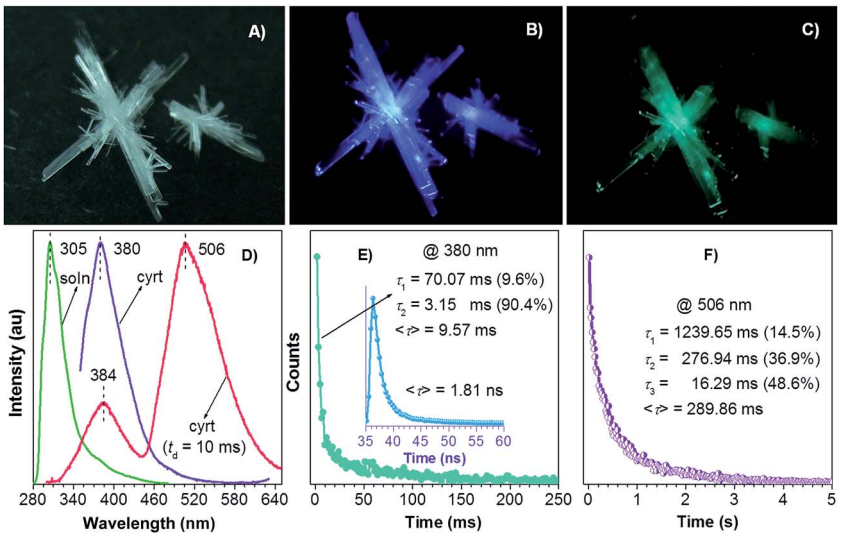

Fig. 2 Photographs of IPA crystals under (A) room light, (B) 365 nm UV light and (C) just after stopping UV light. (D) PL spectra of IPA solution (20 μM in ethanol) and crystals with t_d of 0 and 10 ms. (E) Emission decay curves of IPA crystals monitored at (E) 380 and (F) 506 nm.

the longer one should be ascribed to RTP. Further transient PL measurement demonstrates the $\langle\tau\rangle$ values of prompt fluorescence/RTP for IPA and TFTPA crystals are 1.81 ns/289.86 ms and 0.79 ns/17.93 ms (Fig. 2E, F and 3C), respectively. Meanwhile, besides the ultralong RTP, a durable lifetime of 9.57 ms is also detected for the DF emission of IPA crystals (Fig. 2E).

The above results disclose the CIDE nature of both IPA and TFTPA luminogens. Previously, crystallization-induced emission (CIE, normally fluorescence)[29,30] and CIP[12,21] phenomena were found and developed. However, CIDE for pure organic luminogens, particularly for those without heavy atoms, is virtually an unexplored research area. To gain further insights into the mechanism, crystal structures[31] of the luminogens are investigated. As depicted in Fig. 4, numerous C=O···H–O (1.528, 1.623, 1.703, 2.008, 2.710 Å), C=O···H–C (2.639, 2.688 Å), C=O···O–H (2.581, 2.608, 2.682, 2.857, 2.903 Å), H–O···H–C (2.544 Å), O=C···H–O (2.429, 2.502, 2.573, 2.574 Å), O–H···H–O (2.166, 2.200, 2.280, 2.296 Å), C–H···O–H (2.662 Å), H–O···π (3.154 Å), C–F···H–O (2.647 Å), H–O···H–O (1.746, 2.445 Å) and H–O···O–H (2.558 Å) short contacts, as well as partial edge-to-edge π–π interactions (3.396 Å) are present in the acid crystals, forming two-dimensional (2D, TPA, Fig. 4A) and three-dimensional (3D, IPA and TFTPA, Fig. 4B and S5, ESI†) intermolecular interaction networks. Such abundant and effective interactions firmly lock the molecules and thereby rigidify their conformations. It is also noted that π–π interactions in IPA crystals demonstrate two competitive effects. On the one hand, they may decrease the crystal emission *via* the formation of excimers, however, this adverse effect should be limited because of only small overlaps of the π segments; on the other hand, they contribute to the conformation rigidification, which is favorable for the light emission due to decreased nonradiative dissipations.

Now it becomes clear that in solutions, the excitons of these luminogens are mainly deactivated through nonradiative channels because of the active intramolecular motions (rotations and vibrations) and intermolecular collisions, thus making the luminogenic molecules almost non-emissive. In crystals, however, such intramolecular motions and intermolecular collisions are significantly inhibited due to the

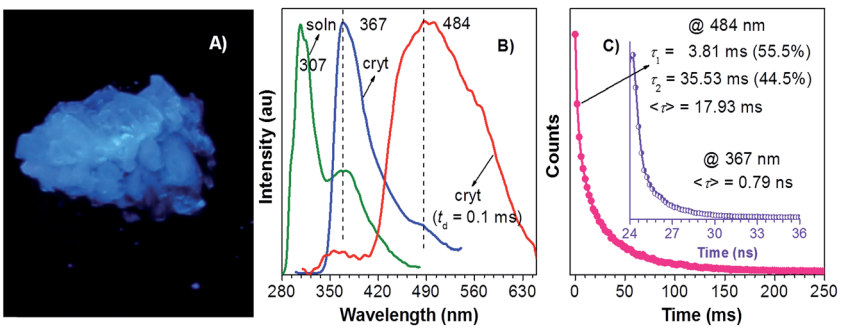

Fig. 3 Photograph of TFTPA crystals under 365 nm UV light. (B) PL spectra of TFTPA solution (20 μM in ethanol) and crystals with t_d of 0 and 0.1 ms. (C) Emission decay curves of TFTPA crystals monitored at 484 and 367 nm (inset).

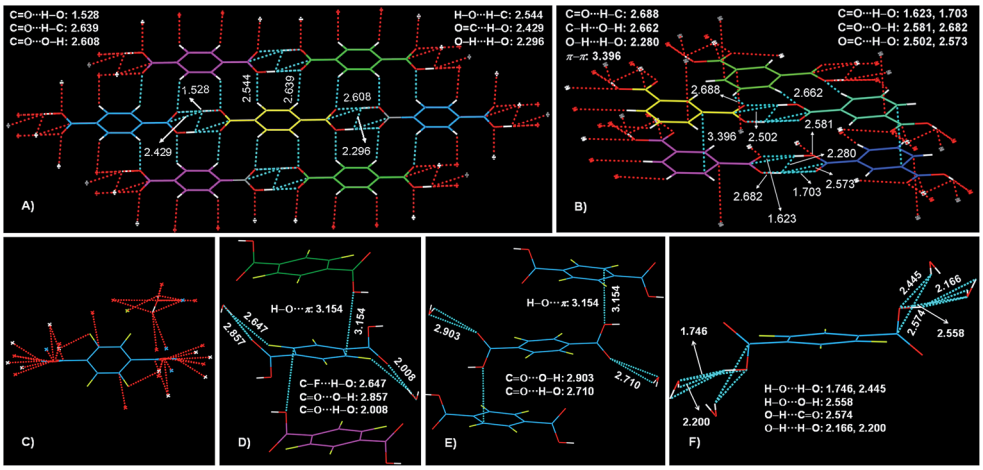

Fig. 4 Perspective view of molecular packing arrangement in (co)crystals of (A) TPA, (B) IPA and (D–F) TFTPA–H_2O. (C) Cocrystal structure of TFTPA–H_2O with multiple intermolecular interactions. Intermolecular interactions are denoted by dotted lines.

conformation rigidification resulting from the efficacious interactions, thus diminishing the radiationless relaxations and boosting the emissions. Such a mechanism is also supported by the cryogenic experiments. As exampled by IPA, when its ethanol solution was frozen by liquid nitrogen (77 K), it gets emissive upon irradiation, also with an afterglow being observed after the stopping of photoexcitation (Video S2, ESI†). Notably, the light emission in frozen solutions is much weaker compared to that in crystals. These results indicate that crystallization performs similarly and even better than the cryogenic conditions that are normally adopted to observe phosphorescence, therefore allowing the observation of phosphorescence at room temperature and alleviating constraints of troublesome cryogenic experiments.

The above results illustrate the CIDE characteristics of proper aromatic acids. Esters are the most common derivatives of acids. Despite the elimination of typical hydrogen bonds in crystals, the presence of carbonyl groups and possible new contacts promoted us to check whether their esters are also CIDE-active. Herein, dimethyl terephthalate (DMTPA) and dimethyl tetrafluoroterephthalate (DMTFTPA) were chosen as the representatives. In analogy to acids, both DMTPA and DMTFTPA do not show any noticeable emissions in ethanol, whose emission maxima/Φ_s values are 320 nm/0.09 ± 0.01% and 347 nm/0.40 ± 0.05%, respectively. The low efficiencies disclose the nonluminescent attribute of both esters in solutions. Under 300 nm UV light irradiation, no visible emission is observed for DMTPA crystals due to their inherent UV light emitting properties (*vide infra*), whereas bright blue light is observed for DMTFTPA crystals (Fig. 5A and B). Further measurements show the PL peaks/Φ_c values of 323 nm/1.5 ± 0.3% and 347, 492 nm/2.7 ± 0.3% for the crystals of DMTPA and DMTFTPA (Fig. 5C and E), respectively, exhibiting remarkable emission enhancement upon crystallization.

The delayed emission spectra (t_d = 0.1 ms) of DMTPA and DMTFTPA crystals show emission peaks at 331/446 and 352/492 nm (Fig. 5C and E), respectively. The former peaks are approaching to those of prompt crystal emissions and solution emissions, proving they are delayed fluorescence, whereas the latter peaks should be assigned to RTP, considering their large Stokes shifts and long $\langle\tau\rangle$ values of ~2.69 (DMTPA) and 9.12 ms (DMTFTPA) (Fig. 5D and F). The mean lifetimes of the prompt fluorescence of both crystals were also determined, giving $\langle\tau\rangle$ values of ~1.17 and 9.12 ns for DMTPA and DMTFTPA,

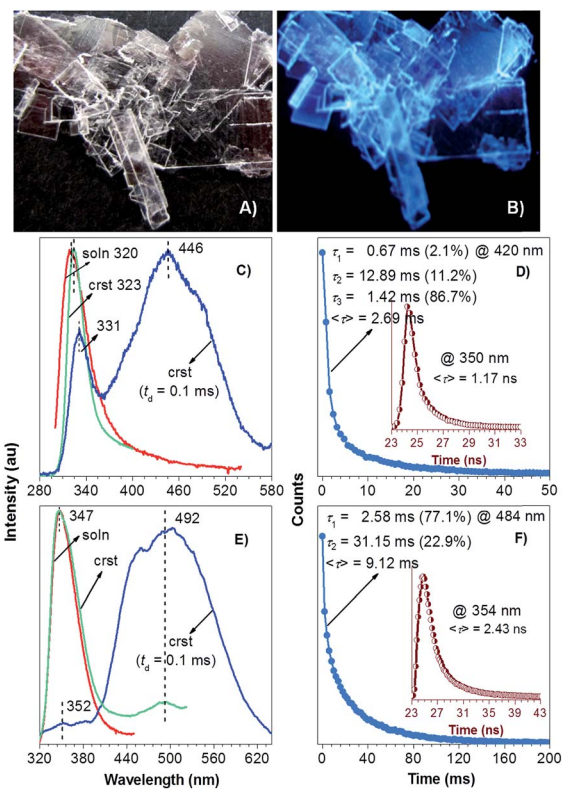

Fig. 5 Photographs of DMTFTPA taken under (A) room light and (B) 300 nm UV light. PL spectra of (C) DMTPA and (E) DMTFTPA solutions (20 μM in ethanol) and crystals with t_d of 0 and 0.1 ms. Emission decay curves of (D) DMTPA and (F) DMTFTPA monitored at 350/420 and 354/484 nm, respectively.

respectively. These results suggest that both ester crystals emit prompt fluorescence, DF and RTP, exhibiting similar CIDE characteristics as their acid parents.

Structure and perspective molecular packing of both crystals are depicted in Fig. 6. Large numbers of C=O···H–C (2.623 Å) and C=O···C–H (3.172 Å) short contacts form a 2D interaction network in DMTPA (Fig. 6A); meanwhile, even more abundant C–F···F–C (2.805 Å), C–F···H–C (2.615 Å), C–F···O–C (2.958 Å), C=O···H–C (2.704 Å) and C=O···π (2.981 Å) intermolecular interactions constitute a firmly locked 3D network (Fig. 6B–E) in DMTFTPA. These effective interactions yield rigidified molecular conformations in crystals, which decrease vibrational dissipations and afford enhanced emissions. Compared to TPA, DMTPA exhibits much lower crystal efficiency, which might be ascribed to the absence of powerful hydrogen bonds. However, DMTFTPA shows similar or even higher crystal efficiency than TFTPA, possibly ascribed to the formation of 3D interaction networks.

To gain more insights into the photophysical processes of the above compounds, theoretical calculations (for computational details, see the ESI†) were conducted. The calculated energy gap and spin–orbit coupling between the involved singlet and triplet states in both gas phases (gas) and crystals (crst) are summarized in Tables S3 and S4 (ESI†). Based on the Franck–Condon principle, the ISC rate is mainly determined by the energy gap and spin–orbit coupling between singlet and triplet states. Small energy gap and large spin–orbit coupling are favorable for the ISC process. Taking TPA for example, for both gas phase and crystal, there are two excited triplet states (T_1 and T_2) lying below the first excited singlet state (S_1), suggesting the possible occurrence of ISCs of $S_1 \leftrightarrow T_1$ and $S_1 \leftrightarrow T_2$. From gas phase to crystal, though the energy gap between S_1 and T_1 ($\Delta E_{S_1T_1}$) is increased from 0.605 to 0.762 eV, that between S_1 and T_2 ($\Delta E_{S_1T_2}$) is significantly decreased from 0.375 to 0.229 eV (Fig. 7, Table S3, ESI†). Moreover, upon crystallization, the spin–orbit coupling between S_1 and T_2 is increased from 4.71 to 11.02 cm^{-1}, far larger than those (*ca.* ≤0.1 cm^{-1}) of hetero-free pure organic molecules. Both above changes indicate ISC and reverse ISC processes become much easier through the effective $S_1 \leftrightarrow T_2$ path in the crystalline state. Meanwhile, the spin–orbit coupling between S_0 and T_1 is also boosted upon crystallization, suggesting more efficient phosphorescence emission. Notably, the oscillator strength is increased by 55 times in crystals compared to that in gas phase, indicating significantly enhanced radiative transition in the crystals. These calculation results agree well with the experimental results.

Photophysical properties of the aromatic acids and esters are summarized in Table 1. Clearly, while they only emit weak fluorescence with fairly low efficiency ($\Phi_s \leq 0.57\%$) in oxygen-free ethanol, they become more emissive in crystals with Φ_c up to 15.3%, giving an enhancement factor (Φ_c/Φ_s) as high as ~46. In solutions (or any other disordered phases), triplet emission is not optimal, and only weak fluorescence from the singlet manifold is generated due to active molecular motions (rotations, vibrations and collisions, Fig. 8A). In crystals, aided by effective intermolecular interactions, molecular conformations become rigidified and molecular motions are significantly hindered, thus making nonradiative deactivations frustrated and subsequently leading to enhanced emissions. Moreover, due to the carbonyl group promoted spin–orbit coupling and singlet–triplet equilibrium, DF and RTP from singlet and triplet manifolds are simultaneously triggered, thus exhibiting CIDE characteristics (Fig. 8B).

Different to strictly fluorescence and purely phosphorescence emitting molecules, such efficient, simultaneous and intrinsic fluorescence and phosphorescence in a single pure organic compound at ambient conditions is unusual and remains virtually unexplored.[19b,32] It not only holds great promise to study dynamic processes and the underlying spin correlations of organic semiconductors within the lifetime of the excitons, but also provides new opportunities for use as optical sensors and attenuators, and spin-independent intermediates for Förster resonant energy transfer.[32,33]

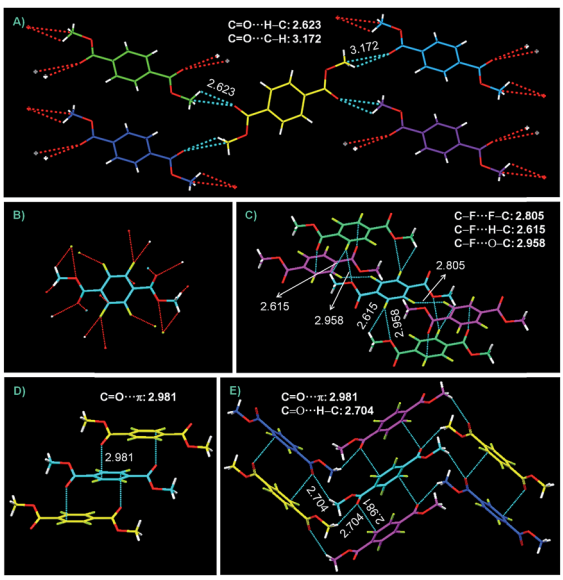

Fig. 6 Perspective view of molecular packing arrangement in crystals of (A) DMTPA and (C–E) DMTFTPA. (B) Crystal structure of DMTPA with multiple intermolecular interactions. Intermolecular interactions are denoted by dotted lines.

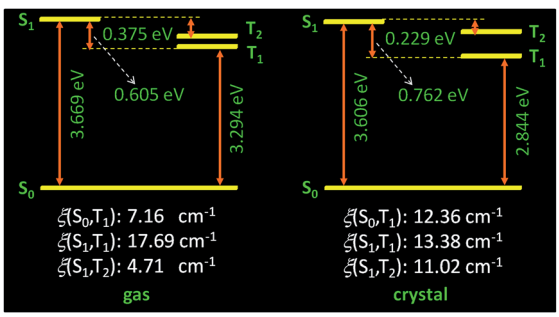

Fig. 7 Calculated energy diagram and spin–orbital coupling of TPA in gas phase (left) and crystalline (right) state.

Table 1 Photophysical properties of aromatic acids and esters[a]

Compound	λ_{ab} (nm)	$\lambda_{em,s}$ (nm)	$\lambda_{em,c}$ (nm)	λ_{delay} (nm)	Φ_s (%)	Φ_c (%)	Φ_c/Φ_s	$\langle\tau\rangle_F$ (ns)	$\langle\tau\rangle_{DF}$ (ms)	$\langle\tau\rangle_P$ (ms)
TPA	235	319	388	392/511	0.57 ± 0.07	8.4 ± 0.3	14.7	0.53	0.16	nd
IPA	228	305	380	384/506	0.33 ± 0.09	15.3 ± 0.3	46.4	1.81	9.57	289.86
TFTPA	221/271	307/367	367	367/484	0.30 ± 0.03	2.0 ± 0.3	6.7	0.79	nd	17.93
DMTPA	240/286/295	320	323	331/446	0.09 ± 0.01	1.5 ± 0.3	16.7	1.17	nd	2.69
DMTFTPA	221/288	347	347/492	352/492	0.40 ± 0.05	2.7 ± 0.3	6.8	2.43	nd	9.12

[a] Ethanol was used to prepare the solutions. Abbreviations: λ_{ab} = absorption peak in solution (concentration = 20 μM, Fig. S6, ESI†), $\lambda_{em,s}$ = emission peak in solution, $\lambda_{em,c}$ = crystal emission peak without delay, λ_{delay} = peak of delayed crystal emission, $\langle\tau\rangle_F$ = lifetime of prompt fluorescence, $\langle\tau\rangle_{DF}$ = lifetime of delayed fluorescence, $\langle\tau\rangle_P$ = lifetime of phosphorescence, nd = not determined.

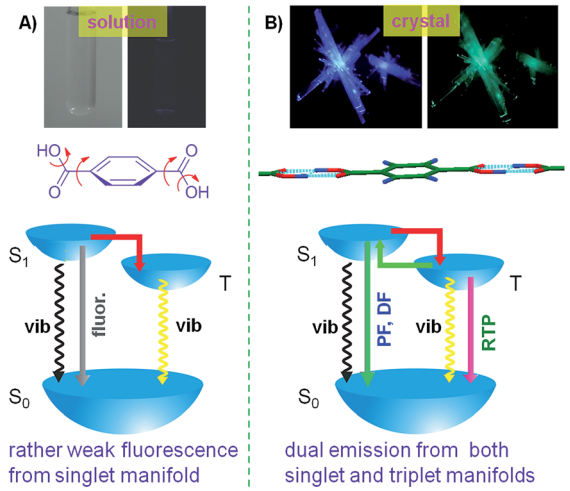

Fig. 8 Schematic illustration of the CIDE phenomenon: (A) highly active molecular motions induced weak fluorescence in solutions and (B) conformation rigidification boosted both fluorescence (prompt and delayed) and phosphorescence in crystals.

It is also noted that the fluorescent emission of the acid crystals are largely red-shifted (up to 75 nm) compared to those in solutions, which should arise from the configuration rigidification and/or dimerization of the molecules. As schematized in the medial part of Fig. 8B, intrinsic intermolecular hydrogen bonds result in the dimers with a more extended planar skeleton. Such a structural feature on one hand increases the rigidity of the molecules, expanding the molecular conjugation; on the other hand may further enhance the electronic delocalization through intermolecular electronic communication, thus resulting in red-shifted emission. For esters, the emissions of crystals and solutions are almost identical owing to the absence of such dimer-like stacking.

Conclusions

In summary, unprecedented CIDE phenomenon in a group of metal- and heavy atom-free aromatic acids and esters is observed under ambient conditions. While carbonyl groups readily promote the ISC processes, these luminogens are actually only faintly fluorescent in solutions due to active molecular motions (rotations, vibrations and collisions). However, they become highly emissive in the crystals due to abundant and effective intermolecular interactions, which rigidify the molecular conformations and diminish the vibrational dissipations. Moreover, besides prompt fluorescence from singlet states, crystallization also triggers simultaneous DF and RTP from the triplet manifold. Specifically, persistent RTP ($\langle\tau\rangle \approx 290$ ms) from IPA crystals is achieved at ambient conditions, which is rarely observed in pure organic luminogens. Such a unique CIDE phenomenon not only provides ideal model systems for fundamental research in revealing the underlying relationships between singlet and triplet states, but also paves the way for developing new materials with RTP and DF for biological (*e.g.* bioimaging and biosensing) and optoelectronic applications.

Acknowledgements

This work was financially supported by the National Natural Science Foundation of China (51473092 and 21104044), the Shanghai Rising-Star Program (15QA1402500) and the National Basic Research Program of China (973 Program, 2013CB834701). Mr Changyun Quan at South China University of Technology is greatly appreciated for the quantum yield measurement of the crystals.

Notes and references

1 (*a*) Y. Ma, H. Zhang, J. Shen and C. Che, *Synth. Met.*, 1998, **94**, 245; (*b*) M. A. Baldo, D. F. O'Brien, Y. You, A. Shoustikov, S. Sibley, M. E. Thompson and S. R. Forrest, *Nature*, 1998, **395**, 151; (*c*) C. Adachi, M. A. Baldo, M. E. Thompson and S. R. Forrest, *J. Appl. Phys.*, 2001, **90**, 5048.

2 (*a*) G. Zhang, G. M. Palmer, M. W. Dewhirst and C. L. Fraser, *Nat. Mater.*, 2009, **8**, 747; (*b*) Y. Han, Y. You, Y. M. Lee and W. Nam, *Adv. Mater.*, 2012, **24**, 2748; (*c*) Y. You, Y. Han, Y.-M. Lee, S. Y. Park, W. Nam and S. J. Lippard, *J. Am. Chem. Soc.*, 2011, **133**, 11488; (*d*) Y. You, S. Lee, T. Kim, K. Ohkubo, W.-S. Chae, S. Fukuzumi, G.-J. Jhon, W. Nam and S. J. Lippard, *J. Am. Chem. Soc.*, 2011, **133**, 18328; (*e*) Q. Zhao, F. Li and C. Huang, *Chem. Soc. Rev.*, 2010, **39**, 3007.

3 (*a*) L. Xiong, Q. Zhao, H. Chen, Y. Wu, Z. Dong, Z. Zhou and F. Li, *Inorg. Chem.*, 2010, **49**, 6402; (*b*) Q. Zhao, M. Yu, L. Shi, S. Liu, C. Li, M. Shi, Z. Zhou, C. Huang and F. Li, *Organometallics*, 2010, **29**, 1085.

4 (*a*) W.-Y. Wong and C.-L. Ho, *Acc. Chem. Res.*, 2010, **43**, 1246; (*b*) C.-L. Lee, I.-W. Hwang, C. C. Byeon, B. H. Kim and N. C. Greenham, *Adv. Funct. Mater.*, 2010, **20**, 2945; (*c*) W. A. Luhman and R. J. Holmes, *Appl. Phys. Lett.*, 2009, **94**, 153304.

5 (*a*) R. C. Evans, P. Douglas and C. J. Winscom, *Coord. Chem. Rev.*, 2006, **250**, 2093; (*b*) V. K.-M. Au, K. M.-C. Wong, D. P.-K. Tsang, M.-Y. Chan, N. Zhu and V. W.-W. Yam, *J. Am. Chem. Soc.*, 2010, **132**, 14273.

6 T. Hofbeck and H. Yersin, *Inorg. Chem.*, 2010, **49**, 9290.

7 (*a*) W. Lu, W.-M. Kwok, C. Ma, C. T.-Z. Chan, M.-X. Zhu and C.-M. Che, *J. Am. Chem. Soc.*, 2011, **133**, 14120; (*b*) N. Komiya, M. Okada, K. Fukumoto, D. Jomori and T. Naota, *J. Am. Chem. Soc.*, 2011, **133**, 6493.

8 (*a*) N. J. Turro, *Modern Molecular Photochemistry*, University Science Books, Sausalito, USA, 1991; (*b*) A. Köhler, J. S. Wilson and R. H. Friend, *Adv. Mater.*, 2002, **14**, 701.

9 E. B. Asafu-Adjaye and S. Y. Su, *Anal. Chem.*, 1986, **58**, 539.

10 A. Sanz-Medel, P. L. Martinez Garcia and M. E. Diaz Garcia, *Anal. Chem.*, 1987, **59**, 774.

11 F. J. DeLuccia and L. J. C. Love, *Anal. Chem.*, 1984, **56**, 2811.

12 W. Z. Yuan, X. Y. Shen, H. Zhao, J. W. Y. Lam, L. Tang, P. Lu, C. Wang, Y. Liu, Z. Wang, Q. Zheng, J. Z. Sun, Y. Ma and B. Z. Tang, *J. Phys. Chem. C*, 2010, **114**, 6090.

13 E. M. Schulman and R. T. Parker, *J. Phys. Chem.*, 1977, **81**, 1932.

14 O. Bolton, K. Lee, H.-J. Kim, K. Y. Lin and J. Kim, *Nat. Chem.*, 2011, **3**, 205.

15 (*a*) H. Y. Gao, X. R. Zhao, H. Wang, X. Pang and W. J. Jin, *Cryst. Growth Des.*, 2012, **12**, 4377; (*b*) H. Y. Gao, Q. J. Shen, X. R. Zhao, X. Q. Yan, X. Pang and W. J. Jin, *J. Mater. Chem.*, 2012, **22**, 5336.

16 (*a*) G. Yong, W. She and Y. Zhang, *Dyes Pigm.*, 2012, **95**, 161; (*b*) G.-P. Yong, Y.-M. Zhang, W.-L. She and Y.-Z. Li, *J. Mater. Chem.*, 2011, **21**, 18520.

17 (*a*) R. Gahlaut, H. C. Joshi, N. K. Joshi, N. Pandey, P. Arora, R. Rautela, K. Suyal and S. Pant, *J. Lumin.*, 2013, **138**, 122; (*b*) M. S. Kwon, D. Lee, S. Seo, J. Jung and J. Kim, *Angew. Chem., Int. Ed.*, 2014, **53**, 11177; (*c*) H. A. Al-Attar and A. P. Monkman, *Adv. Funct. Mater.*, 2012, **22**, 3824.

18 (*a*) Y. Deng, D. Zhao, X. Chen, F. Wang, H. Song and D. Shen, *Chem. Commun.*, 2013, **49**, 5751; (*b*) S. Hirata, K. Totani, J. Zhang, T. Yamashita, H. Kaji, S. R. Marder, T. Watanabe and C. Adachi, *Adv. Funct. Mater.*, 2013, **23**, 3386.

19 (*a*) J. Xu, A. Takai, Y. Kobayashi and M. Takeuchi, *Chem. Commun.*, 2013, **49**, 8447; (*b*) S. Reineke, N. Seidler, S. R. Yost, F. Prins, W. A. Tisdale and M. A. Baldo, *Appl. Phys. Lett.*, 2013, **103**, 093302.

20 X. Zhang, T. Xie, M. Cui, L. Yang, X. Sun, J. Jiang and G. Zhang, *ACS Appl. Mater. Interfaces*, 2014, **6**, 2279.

21 (*a*) Y. Gong, Y. Tan, J. Mei, Y. Zhang, W. Yuan, Y. Zhang, J. Sun and B. Z. Tang, *Sci. China: Chem.*, 2013, **56**, 1178; (*b*) Y. Gong, Y. Tan, H. Li, Y. Zhang, W. Yuan, Y. Zhang, J. Sun and B. Tang, *Sci. China: Chem.*, 2013, **56**, 1183.

22 D. Chaudhuri, E. Sigmund, A. Meyer, L. Röck, P. Klemm, S. Lautenschlager, A. Schmid, S. R. Yost, T. Van Voorhis, S. Bange, S. Höger and J. M. Lupton, *Angew. Chem.*, 2013, **125**, 13691.

23 (*a*) R. H. Friend, R. W. Gymer, A. B. Holms, J. H. Burroughes, R. N. Marks, C. D. Taliani, D. C. Bradley, D. A. Dos Santos, J. L. Brédas, M. Lögdlund and W. R. Salaneck, *Nature*, 1999, **397**, 121; (*b*) A. J. Sandee, C. K. Williams, N. R. Evans, J. E. Davies, C. E. Boothby, A. Köhler, R. H. Friend and A. B. Holmes, *J. Am. Chem. Soc.*, 2004, **126**, 7041.

24 (*a*) D. R. Kearns and W. A. Case, *J. Am. Chem. Soc.*, 1966, **88**, 5087; (*b*) A. A. Lamola and G. S. Hammond, *J. Chem. Phys.*, 1965, **43**, 2129.

25 (*a*) B. H. Meier, F. Graf and R. R. Ernst, *J. Chem. Phys.*, 1982, **76**, 767; (*b*) T. Zhou, F. Li, Y. Fan, W. Song, X. Mu, H. Zhang and Y. Wang, *Chem. Commun.*, 2009, 3199.

26 Herein, Φ_s values were estimated using benzene as standard (Φ_s = 5% in cyclohexane), see: W. R. Dawson and M. W. Windsor, *J. Phys. Chem.*, 1968, **72**, 3251; Φ_c values were determined by a Quantaurus-QY C11347-11 (Hamamatsu, Japan) instrument. For details, see Table S5, ESI†

27 t_d is set according to the instrumental response time and lifetimes of the luminogens. Herein, the emission spectra were obtained on a Perkin-Elmer LS 55 fluorescence spectrometer, for which with $t_d \geq 0.1$ ms, all signals from prompt fluorescence are excluded.

28 (*a*) J. Grzywacz, *Nature*, 1967, **213**, 385; (*b*) K. Nasu, T. Nakagawa, H. Nomura, C.-J. Lin, C.-H. Cheng, M.-R. Tseng, T. Yasuda and C. Adachi, *Chem. Commun.*, 2013, **49**, 10385.

29 (*a*) Y. Dong, J. W. Y. Lam, A. Qin, Z. Li, J. Sun, H. H.-Y. Sung, I. D. Williams and B. Z. Tang, *Chem. Commun.*, 2007, 40; (*b*) L. Qian, B. Tong, J. Shen, J. Shi, J. Zhi, Y. Dong, F. Yang, Y. Dong, J. W. Y. Lam, Y. Liu and B. Z. Tang, *J. Phys. Chem. B*, 2009, **113**, 9098; (*c*) Y. Q. Dong, C. Li, W. Zhao, Y. Dong and B. Z. Tang, *J. Mol. Eng. Mater.*, 2013, **1**, 1340010; (*d*) W. Z. Yuan, Y. Gong, S. Chen, X. Y. Shen, J. W. Y. Lam, P. Lu, Y. Lu, Z. Wang, R. Hu, N. Xie, H. S. Kwok, Y. Zhang, J. Z. Sun and B. Z. Tang, *Chem. Mater.*, 2012, **24**, 1518; (*e*) Y. Lin, G. Chen, L. Zhao, W. Z. Yuan, Y. Zhang and B. Z. Tang, *J. Mater. Chem. C*, 2015, **3**, 112.

30 (*a*) E. Cariati, V. Lanzeni, E. Tordin, R. Ugo, C. Botta, A. G. Schieroni, A. Sironi and D. Pasini, *Phys. Chem. Chem. Phys.*, 2011, **13**, 18005; (*b*) S. Guieu, J. Rocha and A. M. S. Silva, *Tetrahedron*, 2013, **69**, 9329.

31 (*a*) TPA: M. Bailey and C. J. Brown, *Acta Crystallogr.*, 1967, **22**, 387; (*b*) IPA: J. L. Derissen, *Acta Crystallogr.,Sect. B: Struct. Crystallogr. Cryst. Chem.*, 1974, **30**, 2764; (*c*) DMTPA: F. Brisse and S. Perez, *Acta Crystallogr., Sect. B: Struct. Crystallogr. Cryst. Chem.*, 1976, **32**, 2110.

32 S. Reineke and M. A. Baldo, *Sci. Rep.*, 2014, **4**, 3797.

33 S. Reineke and M. A. Baldo, *Phys. Status Solidi A*, 2012, **209**, 2341.

